Assessment of Anisotropic Mechanical Response of Human Skin: Insights from a Clinical Trial

Aflah Elouneg[1*], Arnaud Lejeune[1], Gwenaël Rolin[2, 3, 4], Thomas Lihoreau[4, 5], Brice Chatelain[2], Stéphane Bordas[6], Emmanuelle Jacquet[1*], Jérôme Chambert[1]

[1]Université Marie et Louis Pasteur, CNRS, institut FEMTO-ST, F-25000 Besançon, France.
[2]Université Marie et Louis Pasteur, CHU Besançon, F-25000 Besançon, France.
[3]Université Marie et Louis Pasteur, UMR INSERM 1098 RIGHT, F-25000 Besançon, France.
[4]Université Marie et Louis Pasteur, INSERM CIC1431, F-25000 Besançon, France.
[5]Université Marie et Louis Pasteur, SINERGIES (UR4662), Tech4Health network (F-CRIN),F-25000 Besançon, France .
[6]Institute of Computational Engineering and Sciences, Department of Engineering, Université du Luxembourg, Esch-sur-Alzette, Luxembourg.

*Corresponding author(s). E-mail(s): aflah.elouneg@femto-st.fr; emmanuelle.jacquet@femto-st.fr;

Abstract

This paper presents findings from the SKin Uncertainties Modeling (SKUM) clinical trial aimed at assessing the anisotropic mechanical response of human skin using the annular suction test, employing a numerical method and a commercial device, CutiScan® CS 100. A cohort of 30 healthy volunteers participated in the trial, undergoing in vivo testing on the left forearm through a multi-axial stretch induced by ring suction. Determination of the anisotropy axis was performed using a numerical method based on model fitting of experimental data obtained from oriented elliptic curves, which resulted from the radial deformation of circles. The study evaluates the reproducibility and variability of measurements through an intra-subject study involving five participants, providing insights into the consistency of results within individuals. Additionally, an inter-subject analysis across all subjects offers a comprehensive understanding of anisotropy variability, elucidating broader population tendencies. Furthermore, the study explores correlations between anisotropy and demographic factors such as sex, age, and skin thickness, shedding light on potential influences on skin biomechanics. The analysis showed significant correlations between skin anisotropy and sex, with males displaying a distinct anisotropy axis orientation compared to females. In contrast, no significant associations were found between anisotropy and age among individuals aged 20 to 50, or between anisotropy and epidermal thickness.

Keywords: Skin anisotropy, Multi-axial stretch, *In vivo* measurement, Ring suction test, CutiScan® CS 100

1 Introduction

The influence of mechanical force orientation during the skin repair process has been widely examined since the existence of skin tension lines was reported by Langer in 1861 (Langer, 1861). Historically, surgical incisions on the skin are made parallel to Langer's lines to minimize tension, as incisions generally heal better with less scarring and fibrosis (Wilhelmi et al., 1999). It is known that incisions across Langer's lines are exposed to greater tension and result in more scar tissue formation quantitatively. Therefore, it is recommended that incisions be made along Langer's lines (Aarabi et al., 2007, Son and Harijan, 2014). A significant difference in mechanical response along two perpendicular axes witnesses an orthogonal anisotropic behavior (Reihsner and Menzel, 1996), which could be linked to the density distribution of collagen fibers in both humans (Ridge and Wright, 1966, Gibson et al., 1969, Finlay, 1970, Markenscoff and Yannas, 1979, Annaidh et al., 2012, Ní Annaidh et al., 2012) and animals (Wong et al., 2016, Chen et al., 2020). This highlights the importance of understanding the anisotropic aspect of the mechanical properties of the skin to optimize healing outcomes and minimize scarring.

A multi-axial mechanical load must be applied to the specimen to capture its anisotropic response. For the human skin, the anisotropy has been characterized through different non-invasive methods in the last decades, with optics (Nickell et al., 2000, Sakai et al., 2011), elastography (Gahagnon et al., 2012, Kirby et al., 2022), suction (Tonge et al., 2013, Lakhani et al., 2021), elastic waves (Deroy et al., 2017, Nagle et al., 2023), multi-axial stretch (Reihsner and Menzel, 1996, Gibson et al., 1969, Stark, 1977, Reihsner et al., 1995, Khatyr et al., 2004, Kvistedal and Nielsen, 2007, Verhaegen et al., 2010, Flynn et al., 2011, Boyer et al., 2013, Rosicka et al., 2021). The latter can be conceived as multiple simple in-plane stretch tests conducted in various directions. In addition to the variation in skin stiffness in each direction, the multi-axial test helps identify the anisotropy axis orientation. Nonetheless, this approach is not without limitations. The process of conducting numerous tests to generate load-extension curves in each direction is time-consuming. Conversely, a reduction in the number of angles used to define the direction of minimum extensibility would compromise the accuracy (Serup et al., 2006). Furthermore, applying this technique is not feasible for small skin regions.

A novel commercial device, CutiScan® CS 100 (https://www.courage-khazaka.com/en/scientific-products/cutiscan-cs-100) (hereafter referred to as CutiScan), has been designed to measure the continuous deformation field of soft tissue in all spatial directions within a localized region of 5 mm in diameter. By applying a suction load to an annular surface outside the observed central zone (inner diameter 5 mm, outer diameter 14 mm), the central zone—free from any direct load and designated for measurement—undergoes multi-axial stretching. This deformation enables precise quantification of the angle of the anisotropic axis. It is important to distinguish this technique from the suction test, where the suction load is applied directly to the observed zone (Tonge et al., 2013, Lakhani et al., 2021, Woo et al., 2014, Müller et al., 2018). A similar homemade experimental method was developed in Laiacona *et al.*'s study (Laiacona et al., 2019), but for larger dimensions (inner diameter 30 mm, outer diameter 49 mm). The CutiScan was applied to various body regions, including the forearm (Silva et al., 2019, Elouneg et al., 2022), abdomen (Kim et al., 2020), forehead (Rosado et al., 2015, 2017), leg (Kim et al., 2020, Rosado et al., 2015, 2017), breast (Anthonissen et al., 2022), and earlobe (Elouneg et al., 2020). This widespread usage underscores its effectiveness in capturing anisotropic mechanical responses across different anatomical sites. While the measurement of displacement is generally reliable (Anthonissen et al., 2022), the CutiScan device does have some limitations, as reported in (Elouneg et al., 2020).

One such limitation is that users do not have access to the data of the measured full-field displacement, meaning that the anisotropy axis angle is provided directly by the associated software. Consequently, improving invalidated data is beyond reach. To overcome this limitation, a numerical metho, MARSAC (Multi-Axial Ring Suction Anisotropy Characterization) was developed and validated in (Elouneg et al., 2023). This method utilizes CutiScan's video outputs, which are processed using the Digital Image Correlation (DIC) technique. The displacement field is modeled as a linear isotropic transverse material under radial stretch, incorporating a correction parameter. This approach resulted in an excellent fit between the experimental and model data, accurately representing the position of points of interest after deformation and enabling quantification of the anisotropy axis orientation. The numerical pipeline is publicly accessible at https://github.com/aflahelouneg/MARSAC.

Additionally, in previous studies utilizing the CutiScan (Silva et al., 2019, Kim et al., 2020, Rosado et al., 2017, Anthonissen et al., 2022), the mechanical response of the skin was characterized along only four predetermined axes ($0\,^\circ$, $45\,^\circ$, $90\,^\circ$, $135\,^\circ$). By contrast, the MARSAC-CutiScan system enables the characterization of skin anisotropy in all directions, providing a more comprehensive and detailed analysis.

Overall, this research aims to advance our understanding of the ring suction test in characterizing the anisotropic mechanical properties of human skin along all 360,°. Three main objectives will be addressed: evaluating the reproducibility of the MARSAC-CutiScan system method through within-individual studies, investigating the variability of the anisotropy axis among individuals, and exploring the correlation between anisotropy variability and individuals' age, sex, and skin thickness.

2 Material and Methods

2.1 Clinical Trial

Thirty volunteers (7 males and 23 females, from 18 to 50 yo) were recruited during our clinical study and included at the dermatological department of the University Hospital of Besançon, France. Our trial was registered as SKin Uncertainties Modeling (SKUM) on ClinicalTrial.gov (NCT04995549) and ethically authorized by the French Regulatory Agency (ANSM, reference n°3985309) and ethics committee (Comité de protection des personnes Sud Méditerranée III, reference n° 2020.11.06 20.07.01.37525). All volunteers provided informed consent and our study was conducted in respect of the ethical standards of the Declaration of Helsinki. Among the 30 volunteers, 5 of them benefited from 30 daily skin mechanical measurements for the intra-subject study. 25 volunteers benefited from daily mechanical measurement over 3 consecutive days for the inter-subject analysis. All the biomechanical measurements were performed in a temperature-controlled room (20–22°C, 40–60% relative humidity) after a 15-minute rest period for the patient. The binary categorization (male/female) in this paper refers to the subject's sex, denoting the biological characteristics associated with physical and physiological traits that are assigned at birth. Detailed information about each volunteer is documented in Table 1.

2.2 Skin Thickness Measurement

We used the DUB® SkinScanner75 ultrasound echography system (https://eotech-sa.com/life-science/skin-imaging/dub-skinscanner-2/) to measure the thickness of the epidermis and the dermis. This system employs a probe that emits a frequency wave through a rectangular slot (30 mm × 10 mm) in direct contact with the skin at the mechanical test location.The system operates at a frequency of 22 MHz, providing a penetration depth of 10 mm and a resolution of 72 μm, as specified in the technical datasheet. For clearer visualization of the air-skin interface, the skin surface was moistened with pure water to enhance impedance gradients. The thickness measurement was conducted at the end of the mechanical test (Section 2.3) on the first day to avoid the impact of moisture on the mechanical response.

Figure 1 illustrates the procedures for measuring the thickness of the skin layers. After collecting echography images, the associated software applies phase corrections to flatten the skin surface, thereby simplifying the identification of layer boundaries. Two lines are used to define these boundaries, and the positional difference between the lines represents the thickness of the layers.

2.3 Mechanical Measurement

To capture the anisotropic mechanical response of living human skin, the CutiScan apparatus was configured for use on the left forearm during a clinical trial (Figure 2). It comprises two main parts: a suction probe and a central device. The anatomical

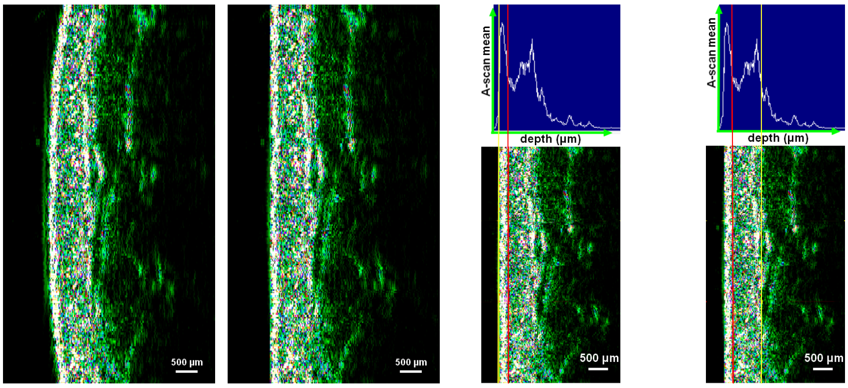

(a) (b) (c) (d)

Fig. 1: Skin layer measurements using the DUB® SkinScanner software. (a) shows a raw echography image of the skin layers obtained from the left forearm of the first volunteer. (b) By enabling phase correction in the software, the air-skin interface is flattened, allowing for uniform thickness measurement. With the help of the A-scan signal (a waveform showing the time and amplitude of the ultrasonic signal), whose average over the measured range is displayed along the vertical axis in the blue graphs (c) and (d), the operator designates the boundaries of the epidermis (c) and dermis (d) layers using red and yellow vertical lines, enabling the measurement of their respective thicknesses. *N.B.* The raw files used for thickness measurements are available at https://dmarc.femto-st.fr/fichiers/821/arborescence.

site, volar left forearm, was chosen because of its easy accessibility and flatness, which facilitates uniform contact between the probe and the skin surface. A standardized protocol has been implemented to improve the reproducibility of the measurements, following the recommendations outlined in a preliminary study (Elouneg et al., 2023). This protocol ensures consistent placement of the probe over the same site, precisely 15 cm from the wrist, used as a reference point, and aligned with the edge of the arm holder. The probe surface needed to be as tangential as possible to the skin to ensure uniform pressure-free contact. A detailed description of the protocol is available in (Elouneg, 2023).

The probe features a black-and-white CCD camera (charge-coupled device) with UV light and applies a constant negative pressure p within an annular area (ring inner and outer diameters of 5 mm and 14 mm, respectively), creating a uniformly in-plane radial stretch in the central zone for 3 seconds. The pressure is then rapidly and completely released during another 3-second phase (Elouneg et al., 2022). The suction pressure can be fixed between 100 mbar and 500 mbar. To secure axisymmetric conditions and isolate the tested site, a double-sided, ring-shaped adhesive was applied around the outer edge of the annular area subjected to suction, having inner and outer diameters of 14 mm and 25 mm, respectively. (see the left-hand part of Figure 2). The probe remained securely adhered to the skin during the entire measurement "series", which consisted of 21 "tests" at pressures ranging from 100 mbar to 500 mbar, in increments of 20 mbar.

A single "test" refers to a complete creep-relaxation cycle lasting 6 seconds. During this process, the in-plane displacement of the material within a circular zone with a 5 mm diameter was recorded using a μEye® camera. The camera, with a resolution of 960×960 pixels, was fixed to the probe, ensuring both were rigidly connected and shared the same reference axes. The probe, along with the fixed camera, was aligned with the axis of the arm holder to maintain consistent orientation throughout the test (see the right-hand part of Figure 2). The output is a video file processed using Digital Image Correlation on the frame at the end of the creep phase ($t = 3$ s), through the Lucas-Kanade method (Lucas and Kanade, 1981), implemented in the Python library PyDIC. Based on a calibration study, the correlation parameters, for instance, window size and grid step size, were set at 72 μm and 20 μm, respectively, with the uncertainty in displacement assessed to be 2%.

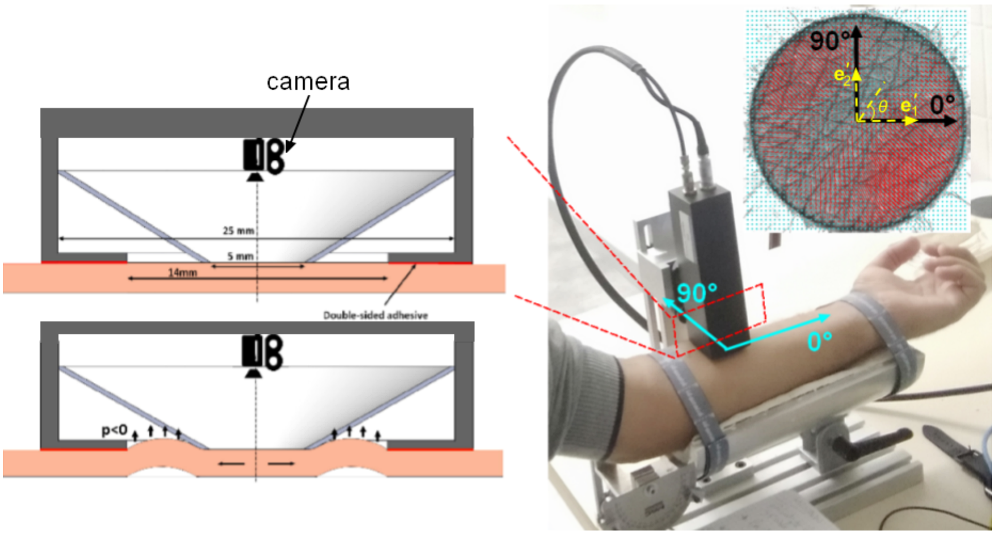

Fig. 2: Experimental setup of the ring suction test conducted on the volar left forearm and illustration of displacement field obtained using the Digital Image Correlation technique (represented by the red lines in the upper right part), applied to video frames recorded by the camera. The reference basis for superimposing the field corresponds to the camera's orientation, with its zero axis aligned with the arm holder axis. The measured site is located along the arm axis, 15 cm from the wrist. The left figure displays a cross-section view of the CutiScan probe before and during suction. Adapted from (Elouneg et al., 2023) and (Elouneg, 2023).

2.4 Anisotropy Axis Identification

Following the method developed in (Elouneg et al., 2023) and introduced in Equation 1, the anisotropy response of a soft tissue subjected to the ring suction load can be characterized by optimizing the mismatch between the experimental data and the model, solved using the Newton-Raphson method. The quantity of interest is the position of the points, $\hat{x}_1^{\mathrm{R}}$ and $\hat{x}_2$, of an ellipse resulting from a deformed circle, whose radius r_{fit} in the undeformed configuration (after setting the probe on the skin and before applying the negative pressure) was set at $r_{\mathrm{fit}} = 1$ mm (Figure 3a). At the convergence of the algorithm, the optimal parameters are obtained: $\boldsymbol{m}_g = \{a, b, \phi\}$ (Figure 3b).

$$\begin{cases} \hat{x}_1^{\mathrm{R}}(r_{\mathrm{fit}}, \theta, a, b, \phi) = a(r_{\mathrm{fit}}) \cos(\theta - \phi) \cos\phi - b(r_{\mathrm{fit}}) \sin(\theta - \phi) \sin\phi \\ \hat{x}_2^{\mathrm{R}}(r_{\mathrm{fit}}, \theta, a, b, \phi) = a(r_{\mathrm{fit}}) \cos(\theta - \phi) \sin\phi + b(r_{\mathrm{fit}}) \sin(\theta - \phi) \cos\phi \end{cases} \quad ; \quad \theta \in [0, 360\,^{\circ}], \tag{1}$$

$\hat{x}_1^{\mathrm{R}}$ and $\hat{x}_2^{\mathrm{R}}$ are the components of the optimal model ellipse points in $\{\boldsymbol{e}_1', \boldsymbol{e}_2'\}$ basis. θ is the angle of a variable axis in the latter basis (Figure 2). a and b are the minor and major semi-axes of the determined ellipse, respectively. ϕ is the angle of the anisotropy axis assumed to be along the minor semi-axis, which is subject to the highest stiffness. ϕ represents the rotation of the model ellipse's semi-axes (expressed in the basis $\{\boldsymbol{e}_1, \boldsymbol{e}_2\}$) with respect to the fixed camera basis $\{\boldsymbol{e}_1', \boldsymbol{e}_2'\}$ (Figure 2) until the best match of the observed ellipse is achieved. The boundary conditions consist of applying radial traction at the edge while fixing the displacement at the central point. The inverse problem and the corresponding model are thoroughly described in (Elouneg et al., 2023). In the present study, we focus on identifying the anisotropy angle, ϕ.

2.5 Data Treatment

The database used in this investigation was organized into three tiers, providing the scientific community with the opportunity to re-analyze the clinical experimental data using alternative methodologies. The public repository, available at https://dmarc.femto-st.fr/depots/134/fichiers (if the server is inaccessible, please contact the corresponding author), grants access to the primary dataset, "`SKUM`," which contains raw files in the form of '.avi' videos captured by the CutiScan device during the clinical trial. Using a Python program stored in the "`SKUM_to_PyDIC`" folder, each video file is segmented into frames and converted into displacement fields. These outputs, referred to as secondary data, are provided as '.csv' tables and '.png' images in the "`PyDIC`" folder, processed through the Digital Image Correlation technique. Finally, the tertiary data consist of the optimal parameters $\boldsymbol{m}_g = a, b, \phi$, which are associated with each mechanical measurement and evaluated using the MARSAC technique. These parameters, along with corresponding illustrations, are archived in the "`MARSAC`" folder. The conversion from secondary to tertiary data is facilitated by another Python program stored in the "`PyDIC_to_MARSAC`" folder.

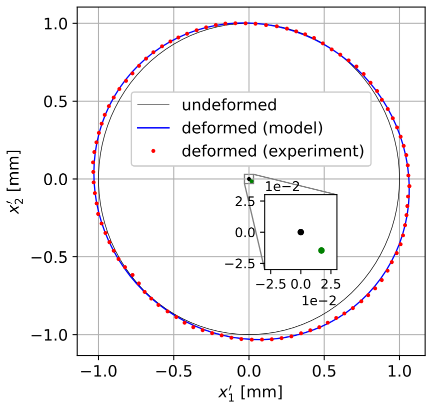

(a) Model fit

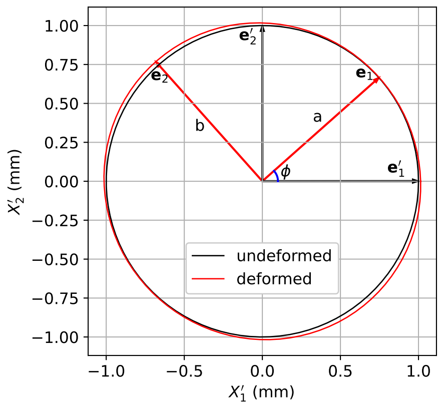

(b) Model parameters

Fig. 3: (a) Fitting observation data with a model ellipse resulting from the deformation of a circle. A correction parameter was added to the model to capture the center shift (from the black to the green dot) and thereby improve the identification. (b) Rotating the model ellipse, with respective parameters $\boldsymbol{m}_g = \{a, b, \phi\}$, to match the experimental data from the deformed circle. The Cartesian coordinate system $\{\boldsymbol{e}'_1, \boldsymbol{e}'_2\}$ corresponds to the fixed probe referential (with $\boldsymbol{e}'_1$ oriented along the forearm holder toward the hand). The model is expressed in the rotating Cartesian coordinate system $\{\boldsymbol{e}_1, \boldsymbol{e}_2\}$. From (Elouneg et al., 2023).

2.6 Statistical Analysis

To evaluate the significance of differences in features such as skin thickness or anisotropy axis orientation between two groups (e.g., male/female or under/above the age of 28), the Student's t-test was employed with a significance level set at 0.05. Prior to applying the t-test Levene's test, Levene's test and the Shapiro-Wilk test were conducted to verify the assumptions of homogeneity of variance and normality, respectively.

A single mechanical measurement series comprises 21 ring suction tests, resulting in 21 identifications of ϕ, enabling the assessment of its reproducibility within each series and for each subject. In total, 225 series were analyzed (30 days $\times 5$ subjects and 3 days $\times 25$ subjects). The standard deviation of each series is denoted as $\mathrm{SD}_{\mathrm{mp}}$ (Standard Deviation Multi-Pressure).

Outliers within each series were identified and removed using the $Z-$test (Seo, 2006), with a confidence level of 95%. Following this, an admissibility check was performed. Initially, if $\mathrm{SD}_{\mathrm{mp}} > 4.5\,°$ (equivalent to 5% uncertainty relative to $180\,°$), the series was deemed irreproducible. However, applying this criterion alone risked discarding many potentially informative and useful measurement series based on visual inspection. To address this, an additional criterion was introduced to reconsider certain initially inadmissible series. If a series exhibited $\mathrm{SD}_{\mathrm{mp}} > 4.5\,°$ but the discrepancy between its median and mean values is less than $4.5\,°$, it is considered acceptable.

3 Results

3.1 Skin Thickness

The findings of the measurements of skin layers' thickness are represented in Figure 4a. The participants were initially arranged by total thickness to highlight variations in skin thickness among individuals and subsequently assigned numbers from 1 to 30. These identifiers will remain consistent throughout the research. Each individual's epidermal and dermal thickness, as well as their sum, are presented along with additional demographic details, for instance, their sex. The t-test was utilized to assess the significance of differences in skin thickness among subjects allocated into two groups based on two distinct factors.

In terms of sex classification, the female group consists of 23 subjects (numbered from 1 to 23), while the male group comprises 7 subjects (ranging from 24 to 30). The results of the t-test indicate p-values below 10^{-4} for total and dermis thickness and 0.78 for epidermis thickness.

In terms of age classification, the initial group comprises 16 subjects under the age of 28, whereas the second group consists of 14 older individuals. Their respective age distributions are 24 ± 2 and 38 ± 7. The p-values associated with total, dermis, and epidermis thicknesses all exceed 0.45, suggesting no significant difference between the two groups. In an alternative approach, we examine the correlation between skin thickness and age using linear regression (Figure 4b). With a correlation coefficient R_{cor} not exceeding 0.02 and p-value above the conventional significance threshold of 0.05, the results suggest that these two variables are uncorrelated among individuals with age from 20 to 50.

3.2 Anisotropy Assessment Reproducibility

Figure 5a shows, as an example, the variability of ϕ over incremental pressure setpoints for three tests conducted on subject 9. The 'Day 1' series represents the median value of $\mathrm{SD}_{\mathrm{mp}}$ among the 225 series. Figure 5b shows the frequency distribution of the measurement series as a function of $\mathrm{SD}_{\mathrm{mp}}$. The results show that 15% of the series had a variability of less than 1°, 50% less than 2°, 69% less than 3°, and 84% less than 4.5°. If a maximum $\mathrm{SD}_{\mathrm{mp}}$ of 4.5° is accepted, 16% of the series would be eliminated following the first criterion established in Section 2.6, preliminarily applied. The remaining 16% were reexamined within the alternative criterion. Consequently, only 3 out of 225 tests were excluded from subsequent analyses. In the following sections, a reproducible set of 21 pressure levels will be represented by their mean values. All values are provided in the Appendix (Tables 2, 3, and 4).

3.3 Within-subject variability

The 5 subjects $\{12, 13, 24, 26, 30\}$, labeled in this within-subject variability study $\{S_{\mathrm{w}1}, S_{\mathrm{w}2}, S_{\mathrm{w}3}, S_{\mathrm{w}4}, S_{\mathrm{w}5}\}$, respectively, participated in 30 series of mechanical measurements. Once inadmissible sets were excluded (3 out of 225: 'Day 1' and 'Day 12' for $S_{\mathrm{w}1}$ and 'Day 24' for $S_{\mathrm{w}5}$), the day-to-day variability of the anisotropy axis was

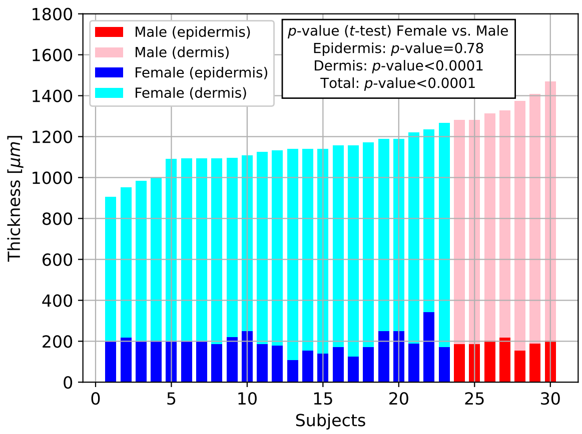

(a)

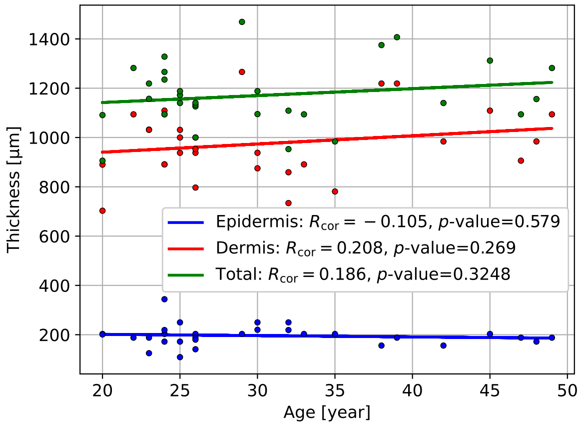

(b)

Fig. 4: (a) Variability in skin layer thickness across subjects. (b) Linear regression of skin layer thickness with respect to subjects' age, where R_{cor} denotes the Pearson correlation coefficient.

evaluated for each subject (Figure 6). As a result, at least 28 sets were required to achieve the maximum uncertainty of $10.42\,^{\circ}$ (double side) around the anisotropy axis.

3.4 Between-subject variability

25 subjects participated in the series of ring suction tests three times each. All 75 series met the reproducibility criteria described in Section 2.6. The identified anisotropy axes are grouped together with the averaged values for the subjects $12, 13, 24, 26, 30$ from the within-subject study, which included around 30 sets per subject. Assume that the means of 3 measurement series can represent the average of 30 measurement series

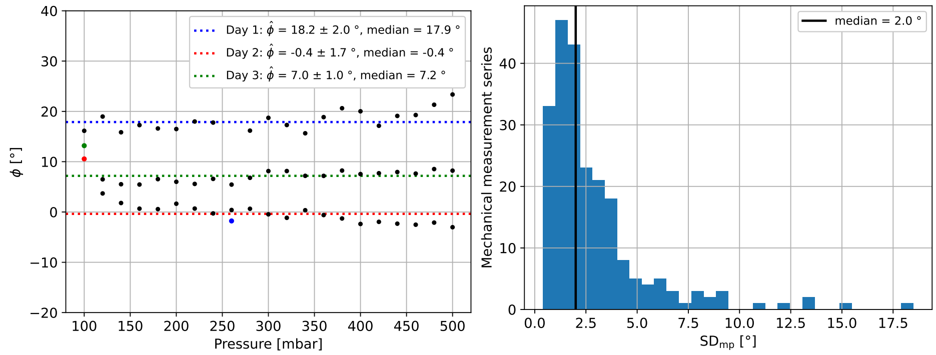

(a) (b)

Fig. 5: (a) Quantification of anisotropy variability over one set of mechanical measurements for subject 9. $\hat{\phi}$ is the average of ϕ over different pressure levels. Using the Z-score method with a 95% confidence level, 3 outliers were excluded: 260 mbar for 'Day 1' (blue dot), and 100 mbar for both 'Day 2' (red dot) and 'Day 3' (green dot). (b) Counts of the measurement sets (all subjects combined) as a function of their respective anisotropy assessment variability (SD_{mp} value of all subjects are provided in the Appendix: Tables 2, 3, and 4).

with a 5% uncertainty. Consequently, these means are treated as single data points for each subject in the analysis of variability based on factors such as sex, age, and skin thickness. This hypothesis was further explored in a supplementary study (Figure 9).

Starting with the factor of skin thickness, the anisotropy axis was compared to the thickness of the epidermis and dermis, as well as their combined thickness, as shown in Figure 7a. Linear regression was performed for each case and the correlation between the variables was quantified using R_{cor}. The correlation between epidermis thickness and anisotropy angle was found to be insignificant, indicated by a low R_{cor} and confirmed by a $p-$value > 0.05, in contrast to the dermis and total thickness. In the case of the latter, a coefficient of R_{cor} higher than 0.5 would suggest a relationship between dermis thickness and skin anisotropy, although further examination is needed for a comprehensive understanding.

As for the age, Figure 7b illustrates a near complete lack of linear correlation with the anisotropy axis ($R_{\text{cor}} \approx 0$ and $p-$value ≈ 1), suggesting that the anisotropy of the skin remains unaffected by the aging process for individuals in the age range of $20-50$.

The uncountable nature of the sex factor necessitates in the examination of its impact on skin anisotropy an evaluation of the significance of the disparity between male and female samples. Various statistical tests were conducted for this purpose, including the independent Student's test (commonly referred to as the t-test), Levene's test, and Shapiro-Wilk's test. Following confirmation of normal distribution for both sets of samples, as indicated by Shapiro-Wilk's test yielding a p-value greater than 0.59 for each group, and verification of homogeneous variances through Levene's test with a p-value exceeding 0.94, the independent t-test was executed using the Python library

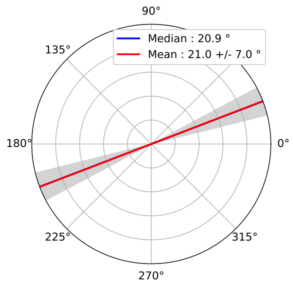

(a) $S_{\mathrm{w}1}$

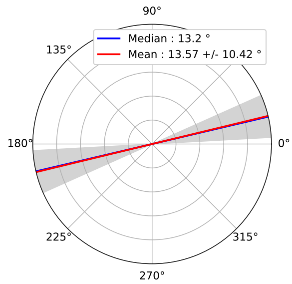

(b) $S_{\mathrm{w}2}$

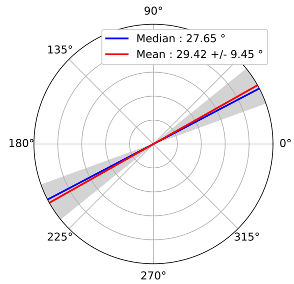

(c) $S_{\mathrm{w}3}$

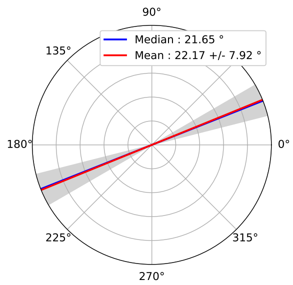

(d) $S_{\mathrm{w}4}$

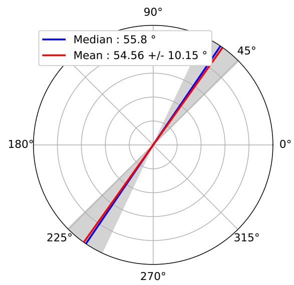

(e) $S_{\mathrm{w}5}$

Fig. 6: Within-subject variability of the anisotropy axis orientation for five subjects is displayed on the $\{\boldsymbol{e}'_1, \boldsymbol{e}'_2\}$ basis. Each subfigure shows the mean anisotropy axis, ϕ, averaged over 30 mechanical measurement series, except for the subjects $S_{\mathrm{w}1}$ (28 series) $S_{\mathrm{w}5}$ (29 series). The gray zones represent the 95% confidence interval, with the opening angle corresponding to the standard deviation.

`scipy`. The results revealed a p-value below 0.005, indicating a significant distinction in the anisotropy axis between males and females (Figure 8).

A similar methodology was employed when examining the age variable, despite its quantifiability. The statistical evaluation of the discrepancy between the groups under and over 28 years old was conducted. The normality assessment indicated a p-value exceeding 0.48, while the p-value associated with the test for variance equality was 0.22. Subsequently, the application of the t-test demonstrated that the differences between the two groups were not deemed statistically significant (Figure 8).

4 Discussions

In this section, we interpret the results according to the four main themes outlined in Section 3: variability of skin thickness, reproducibility of the anisotropy assessment method, and variability of anisotropy both within and between subjects.

The results presented in Section 3.1 and Figure 4a highlight two key findings: males have thicker dermis compared to females, while no significant difference in epidermis thickness was observed between the two groups. These findings are consistent

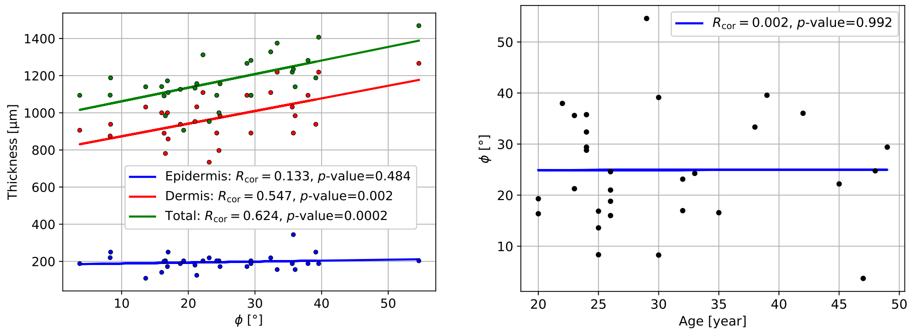

(a) (b)

Fig. 7: Linear regression to examine the relationship between the anisotropy angle and two variables, namely (a) skin thickness and (b) age. R_{cor} stands for the Pearson's correlation coefficient, while the p-value is linked to the null hypothesis stating the absence of a linear relationship.

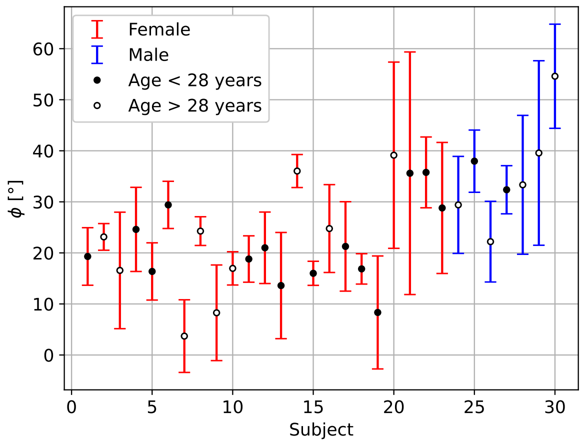

Fig. 8: Between-subject variability of the skin anisotropy angle. The independent t-test was performed to evaluate the statistical discrepancy between groups, Female *vs.* Male with p-value $= 0.021$, under *vs.* over 28 years old with p-value $= 0.46$.

with those reported in Rahrovan *et al.*'s study (Rahrovan et al., 2018) and can be explained by observations in (Dao and Kazin, 2007), which suggest that dermis thickness may correlate with collagen content, influenced by hormonal factors. Specifically, males typically have higher levels of testosterone, which contributes to thicker skin. In contrast, the epidermis lacks collagen fibers, accounting for the absence of thickness differences in this layer.

According to Leveque *et al.* (Leveque et al., 1984), the reduction in skin thickness due to aging commences at the age of 45 for both males and females. In contrast, Shuster *et al.* (Shuster et al., 1975) found that skin thickness decreases linearly in males from the age of 20, while it remains constant in females until around 50 years. Our analysis did not detect any significant difference between individuals below and above 28 years old (with a p-value greater than 0.45 for both layers and their combination). Additionally, as illustrated in Figure 4b, there was no observable linear relationship between age and the first two layers of skin. Consequently, the impact of aging on skin thickness is negligible for individuals between 20 and 50 years old. It is noteworthy that the total thickness, which comprises the epidermis and dermis, exhibits a similar trend to the dermis, as the proportion of the latter accounts for approximately 83%.

The second subject focuses on studying the reproducibility of the experimental setup, which utilizes a CutiScan probe, in conjunction with a numerical method referred to as MARSAC for the evaluation of skin anisotropy *in vivo*. For each of the 225 mechanical measurement series, the mean, standard deviation, and median were calculated, as illustrated in Figure 5a and reported in Tables 2, 3, and 4.

Using the statistical criterion $SD_{\mathrm{mp}} \leq 4.5\,^{\circ}$, the system's reproducibility was determined to be 84%, as shown in Figure 5b. This result indicates that the anisotropy axis remains stable despite a gradual increase in suction pressure. For the remaining 16%, a reexamination using an alternative criterion identified additional acceptable series, resulting in only 3 out of 225 series being rejected. The significant discrepancies observed in these discarded series could be attributed to factors such as variations in camera brightness within the probe, instability in the participant's position during the 40-minute measurement series, or excessive pressure exerted by the probe on the skin. Following this reproducibility study, we propose reducing the number of tests per series and focusing them around the median pressure of 300 mbar. This adjustment would shorten the experiment duration, improving efficiency and potentially encouraging greater participation in future studies.

The variability of the skin anisotropy axis within a single subject was explored. Due to the considerable amount of data required, the study was conducted on 5 subjects with 30 series each. As depicted in Figure 6, changes in ϕ over 30 days showed that each subject's left forearm has a specific anisotropy axis with an uncertainty ranging from $14\,^{\circ}$ to $20\,^{\circ}$. Given the materials and methods of the study, identifying the sources of this uncertainty is challenging. The observed variability may be due to the lack of protocol robustness (irregularity of personal habits, such as sport paractice, uncustomized arm support, ...) or daily changes in skin mechanical properties, as suggested in (Olsen and Jemec, 1993). The latter reports that significant changes were observed as early as 10 minutes after the application of water and paraffin oil. Additionally, comparing this uncertainty with previous works that used the CutiScan (Silva et al., 2019, Kim et al., 2020, Rosado et al., 2017, Anthonissen et al., 2022) is not entirely accurate, as those studies characterized the mechanical response along only 4 predetermined axes ($0\,^{\circ}$, $45\,^{\circ}$, $90\,^{\circ}$, $135\,^{\circ}$). In contrast, this study is the first clinical trial to employ the CutiScan for precisely identifying the anisotropy axis orientation through full-field displacement data analysis.

Considering that 3 acceptable series could potentially result in the identification of the specific anisotropy axis of an individual, the evaluation of ϕ was conducted on a cohort of 25 subjects, each undergoing 3 tests. To verify that 3 measurement series are sufficient to provide representative information, the means from a full set of 30 series were compared with the means from subsets comprising the first n measurement series, where $n = 2, 3, ..., 29$. The results for all 5 subjects, summarized in the Appendix (Figure 9), indicate that the chosen number of 3 measurement series per subject in the between-subject study is appropriate, with a maximum error of 5%.

Through the utilization of linear regression analysis on ϕ concerning quantifiable factors such as skin thickness and age (depicted in Figure 7), it is observed that the anisotropy of the skin is not influenced by the thickness of the epidermis (Figure 7a) or the age of the individual (Figure 7b). Demonstrating a correlation coefficient exceeding 0.5 and a p-value of 0.002, the relationship between dermis thickness and ϕ can be classified as moderately significant (Taylor, 1990). Interpreting the linear relationship solely based on the correlation coefficient is inadequate without considering the context of the study. In certain instances, the observed R_{cor} might be low to data point dispersion rather than a lack of correlation strength. Upon closer examination of Figure 7a, an intuitive assumption of the correlation between dermis thickness and the anisotropy axis can be made. Further elaboration on this phenomenon is provided further in this section.

Referring to the data presented in Figure 8, error bars were used to illustrate the variation of ϕ over a span of 3 days in conjunction with the data pertaining to the subjects {12, 13, 24, 26, 30} (primarily consisting of 30 tests). The analysis reveals discernible tendencies in the orientation of the anisotropy axis among female participants (approximately $20\,^{\circ}$) and male participants (around $40\,^{\circ}$), albeit no significant disparities were observed among groups categorized by age, specifically those below and above 28 years old. In order to substantiate this conjecture, an independent samples t-test was conducted to compare the two groups based on their sex and age. As the resulting p value falls below the conventional significance threshold, it would affirm the existence of a statistically significant difference in the orientation of the anisotropy axis between female and male individuals. Comparing these results with existing literature would provide a valuable context. However, to the best of the authors' knowledge, sex-dependent anisotropy behavior has been minimally studied (Gräßel et al., 2005, Lin et al., 2024), and not specifically in the human forearm.

The disparity in the thickness of the dermis observed between males and females, along with its relationship to the anisotropy axis, raises the possibility of a correlation between sex and the anisotropy axis. In addition, the introduction highlighted that the orientation of skin anisotropy is governed by the distribution of collagen within the dermis. An increased thickness of the dermis is known to correspond to a higher concentration of collagen fibers (Shuster et al., 1975), prompting speculation that their predominant orientation is influenced by their density. This statement holds true under two key assumptions: (1) the thickness of the epidermis remains constant, and (2) the epidermis exhibits anisotropic properties. Under these conditions, changes in the epidermis-to-dermis thickness ratio would influence the global anisotropy axis orientation. To illustrate that, a numerical simulation is presented in the Appendix (Figure 11). To the best of the authors' knowledge, a study of this nature has not yet been undertaken. Therefore, it would be advantageous to replicate a similar investigation with additional data collection, specifically focusing on aspects such as the nesting of collagen fibers before and after the ring suction test, as well as incorporating dimensions relevant to the specific site under examination, such as the circumferences of the wrist, middle arm, and elbow.

The current work has some limitations that warrant future exploration and clarification. First, the strength of anisotropy is considered as the ratio of the displacement along and across the anisotropy axis, specifically $\frac{a-r_{\text{fit}}}{b-r_{\text{fit}}}$. This ratio is crucial for assessing the state of anisotropy. However, accurately determining this ratio presents challenges. Specifically, the displacement along the stiffer direction is very small, often falling within the measurement noise level, which makes assessing the strength of anisotropy highly uncertain, as discussed in (Elouneg et al., 2023). Despite this, it is important to note that significant variability in this ratio is uncorrelated with the anisotropy axis angle ϕ, based on the reported fitting solution for each volunteer in (Elouneg, 2023). Second, the potential influence of friction between the probe and the skin on the identification of the anisotropy axis angle merits consideration. As reported in (Elouneg et al., 2022), in a specific case, the findings demonstrated a minimal impact of friction on the probe's return position after relaxation, with angular independence consistently observed in the measurements. Nevertheless, we acknowledge that inhomogeneous friction—potentially influenced by variations in skin texture—could affect the deviation of the anisotropy axis. This aspect was not specifically investigated in the present study and represents an opportunity for future research. Finally, we discuss a limitation related to the issue of sex parity in the clinical trial. The sample size consists of 23 females and 7 males, introducing uncertainty regarding the reproducibility of the significant difference of ϕ between the two groups. This issue has been addressed through a supplementary analysis, detailed in Figure 10. Nonetheless, enhancing the inclusion of males in the research study would lead to more conclusive findings.

5 Conclusion

This study presents a detailed investigation into the anisotropic mechanical properties of human skin using a numerical-based methodology and the commercial device, CutiScan® CS 100. Through in vivo testing on a cohort of 30 subjects, we explored the reproducibility and variability of skin anisotropy measurements and examined correlations with demographic factors such as sex, age, and skin thickness. Analysis revealed significant correlations between skin anisotropy and sex. Notably, males exhibited a different anisotropy axis orientation compared to females, potentially linked to differences in dermis thickness and collagen distribution. However, no significant relationship was found between anisotropy and age for individuals between 20 and 50, nor between anisotropy and epidermal thickness. To build on these findings, future research should focus on larger, more diverse cohorts and incorporate additional factors such as collagen fiber morphology and site-specific dimensions.

Acknowledgements. This work was conducted within the framework of the EIPHI Graduate School (contract ANR-17-EURE-0002). It was supported by the French Agence Nationale de la Recherche (ANR) grant (No. ANR-21-CE45-0025), the Région de Bourgogne Franche-Comté, France (grant No. 2018-Y-07543), and the Luxembourg National Research Fund (OTP S-STR-8001-00-B). The authors acknowledge the contribution of Intissar Ben Moussa to the clinical trial during her internship.

References

Langer, K.: Zue anatomie und physiologie de haut. ueber der spaltbarkeit der cutis. Sitzungsberich der Academie der Wissenschaften in Wien **44**(19), 1861 (1861)

Wilhelmi, B.J., Blackwell, S.J., Phillips, L.G.: Langer's lines: to use or not to use. Plastic and Reconstructive Surgery **104**(1), 208–214 (1999) https://doi.org/10.1097/00006534-199907000-00033

Aarabi, S., Bhatt, K.A., Shi, Y., Paterno, J., Chang, E.I., Loh, S.A., Holmes, J.W., Longaker, M.T., Yee, H., Gurtner, G.C.: Mechanical load initiates hypertrophic scar formation through decreased cellular apoptosis. The FASEB Journal **21**(12), 3250–3261 (2007) https://doi.org/10.1096/fj.07-8218com

Son, D., Harijan, A.: Overview of surgical scar prevention and management. Journal of Korean Medical Science **29**(6), 751–757 (2014) https://doi.org/10.3346/jkms.2014.29.6.751

Reihsner, R., Menzel, E.: On the orthogonal anisotropy of human skin as a function of anatomical region. Connective Tissue Research **34**(2), 145–160 (1996) https://doi.org/10.3109/03008209609021498

Ridge, M.D., Wright, V.: The directional effects of skin: A bio-engineering study of skin with particular reference to Langer's lines. Journal of Investigative Dermatology **46**(4), 341–346 (1966) https://doi.org/10.1038/jid.1966.54

Gibson, T., Stark, H., Evans, J.: Directional variation in extensibility of human skin in vivo. Journal of Biomechanics **2**(2), 201–204 (1969) https://doi.org/10.1016/0021-9290(69)90032-3

Finlay, J.B.: Biodynamic studies of human skin: torsional characteristics in relation to structure. PhD thesis, University of Strathclyde (1970)

Markenscoff, X., Yannas, I.V.: On the stress-strain relation for skin. Journal of Biomechanics **12**(2), 127–129 (1979) https://doi.org/10.1016/0021-9290(79)90151-9

Annaidh, A.N., Bruyère, K., Destrade, M., Gilchrist, M.D., Otténio, M.: Characterization of the anisotropic mechanical properties of excised human skin. Journal of the Mechanical Behavior of Biomedical Materials **5**(1), 139–148 (2012) https://doi.org/10.1016/j.jmbbm.2011.08.016

Ní Annaidh, A., Bruyère, K., Destrade, M., Gilchrist, M.D., Maurini, C., Otténio, M., Saccomandi, G.: Automated estimation of collagen fibre dispersion in the dermis and its contribution to the anisotropic behaviour of skin. Annals of Biomedical Engineering **40**(8), 1666–1678 (2012) https://doi.org/10.1007/s10439-012-0542-3

Wong, W., Joyce, T., Goh, K.: Resolving the viscoelasticity and anisotropy dependence of the mechanical properties of skin from a porcine model. Biomechanics and modeling in mechanobiology **15**(2), 433–446 (2016) https://doi.org/10.1007/s10237-015-0700-2

Chen, S., Ní Annaidh, A., Roccabianca, S.: A microstructurally inspired constitutive model for skin mechanics. Biomechanics and modeling in mechanobiology **19**, 275–289 (2020) https://doi.org/10.1007/s10237-019-01210-9

Nickell, S., Hermann, M., Essenpreis, M., Farrell, T.J., Krämer, U., Patterson, M.S.: Anisotropy of light propagation in human skin. Physics in Medicine and Biology **45**(10), 2873–2886 (2000) https://doi.org/10.1088/0031-9155/45/10/310

Sakai, S., Yamanari, M., Lim, Y., Nakagawa, N., Yasuno, Y.: In vivo evaluation of human skin anisotropy by polarization-sensitive optical coherence tomography. Biomedical Optics Express **2**(9), 2623–2631 (2011) https://doi.org/10.1364/BOE.2.002623

Gahagnon, S., Mofid, Y., Josse, G., Ossant, F.: Skin anisotropy in vivo and initial natural stress effect: A quantitative study using high-frequency static elastography. Journal of Biomechanics **45**(16), 2860–2865 (2012) https://doi.org/10.1016/j.jbiomech.2012.08.032

Kirby, M.A., Tang, P., Liou, H.-C., Kuriakose, M., Pitre, J.J., Pham, T.N., Ettinger, R.E., Wang, R.K., O'Donnell, M., Pelivanov, I.: Probing elastic anisotropy of human skin in vivo with light using non-contact acoustic micro-tapping oce and polarization sensitive oct. Scientific Reports **12**(1), 1–17 (2022) https://doi.org/10.1038/s41598-022-07775-3

Tonge, T.K., Atlan, L.S., Voo, L.M., Nguyen, T.D.: Full-field bulge test for planar anisotropic tissues: Part i – experimental methods applied to human skin tissue. Acta Biomaterialia **9**(4), 5913–5925 (2013) https://doi.org/10.1016/j.actbio.2012.11.035

Lakhani, P., Dwivedi, K., Parashar, A., Kumar, N.: Non-invasive in vivo quantification of directional dependent variation in mechanical properties for human skin. Frontiers in Bioengineering and Biotechnology **9**, 749492 (2021) https://doi.org/10.3389/fbioe.2021.749492

Deroy, C., Destrade, M., Mc Alinden, A., Ní Annaidh, A.: Non-invasive evaluation of skin tension lines with elastic waves. Skin Research and Technology **23**(3), 326–335 (2017) https://doi.org/10.1111/srt.12339

Nagle, M., Price, S., Trotta, A., Destrade, M., Fop, M., Ní Annaidh, A.: Analysis of in vivo skin anisotropy using elastic wave measurements and bayesian modelling. Annals of biomedical engineering **51** (2023) https://doi.org/10.1007/s10439-023-03185-2

Stark, H.L.: Directional variations in the extensibility of human skin. British Journal of Plastic Surgery **30**(2), 105–114 (1977) https://doi.org/10.1016/0007-1226(77)90001-7

Reihsner, R., Balogh, B., Menzel, E.: Two-dimensional elastic properties of human skin in terms of an incremental model at the in vivo configuration. Medical Engineering & Physics **17**(4), 304–313 (1995) https://doi.org/10.1016/1350-4533(95)90856-7

Khatyr, F., Imberdis, C., Vescovo, P., Varchon, D., Lagarde, J.-M.: Model of the viscoelastic behaviour of skin in vivo and study of anisotropy. Skin Research and Technology **10**(2), 96–103 (2004) https://doi.org/10.1111/j.1600-0846.2004.00057.x https://onlinelibrary.wiley.com/doi/pdf/10.1111/j.1600-0846.2004.00057.x

Kvistedal, Y.A., Nielsen, P.M.F.: Estimating material parameters of human skin in vivo. Biomechanics and Modeling in Mechanobiology **8**(1), 1–8 (2007) https://doi.org/10.1007/s10237-007-0112-z

Verhaegen, P.D., Res, E.M., Van Engelen, A., Middelkoop, E., Van Zuijlen, P.P.: A reliable, non-invasive measurement tool for anisotropy in normal skin and scar tissue. Skin Research and Technology **16**(3), 325–331 (2010) https://doi.org/10.1111/j.1600-0846.2010.00436.x

Flynn, C., Taberner, A., Nielsen, P.: Mechanical characterisation of in vivo human skin using a 3d force-sensitive micro-robot and finite element analysis. Biomechanics and Modeling in Mechanobiology **10**(1), 27–38 (2011) https://doi.org/10.1111/j.1600-0846.2010.00436.x

Boyer, G., Molimard, J., Tkaya, M.B., Zahouani, H., Pericoi, M., Avril, S.: Assessment of the in-plane biomechanical properties of human skin using a finite element model updating approach combined with an optical full-field measurement on a new tensile device. Journal of the Mechanical Behavior of Biomedical Materials **27**, 273–282 (2013) https://doi.org/10.1016/j.jmbbm.2013.05.024

Rosicka, K., Hill, M., Wdowski, M.: Skin anisotropy: Finding the optimal incision line for volar forearm in males and females. Journal of the Mechanical Behavior of Biomedical Materials **124**, 104805 (2021) https://doi.org/10.1016/j.jmbbm.2021.104805

Serup, J., Jemec, G.B., Grove, G.L.: Handbook of Non-Invasive Methods and the Skin. CRC Press, Boca Raton (2006). https://doi.org/10.3109/9781420003307

Woo, M., Moon, K., Jung, H., Park, S., Moon, T., Kim, N., Lee, B.: Comparison of skin elasticity test results from the ballistometer® and cutometer®. Skin Research and Technology **20**(4), 422–428 (2014) https://doi.org/10.1111/srt.12134

Müller, B., Elrod, J., Pensalfini, M., Hopf, R., Distler, O., Schiestl, C., Mazza, E.: A novel ultra-light suction device for mechanical characterization of skin. PLOS One **13**(8), 1–22 (2018) https://doi.org/10.1371/journal.pone.0201440

Laiacona, D., Cohen, J.M., Coulon, K., Lipsky, Z.W., Maiorana, C., Boltyanskiy, R., Dufresne, E.R., German, G.K.: Non-invasive in vivo quantification of human skin tension lines. Acta Biomaterialia **88**, 141–148 (2019) https://doi.org/10.1016/j.actbio.2019.02.003

Silva, H., Francisco, R., Rodrigues, L.: Texture analysis is a useful tool to characterize the cutaneous biomechanical profile: A análise de textura é uma ferramenta útil para caracterizar o perfil biomecânico cutâneo. Journal Biomedical and Biopharmaceutical Research **16**, 188–194 (2019) https://doi.org/10.19277/bbr.16.2.211

Elouneg, A., Bertin, A., Lucot, Q., Tissot, V., Jacquet, E., Chambert, J., Lejeune, A.: In vivo skin anisotropy dataset from annular suction test. Data in Brief **40**, 107835 (2022) https://doi.org/10.1016/j.dib.2022.107835

Kim, M.A., Jung, Y.C., Kim, E.J.: Evaluation of anisotropic properties of striae distensae with regard to skin surface texture and viscoelasticity. Skin Research and Technology **26**(2), 220–225 (2020) https://doi.org/10.1111/srt.12783

Rosado, C., Antunes, F., Barbosa, R., Fernando, R., Rodrigues, L.M.: Cutiscan®-a new system of biomechanical evaluation of the skin in vivo-comparative study of use depending on the anatomical site. Biomedical and Biopharmaceutical Research **12**(1), 49–57 (2015) https://doi.org/10.19277/bbr.12.1.103

Rosado, C., Antunes, F., Barbosa, R., Fernando, R., Estudante, M., Silva, H.N., Rodrigues, L.M.: About the in vivo quantitation of skin anisotropy. Skin Research and Technology **23**(3), 429–436 (2017) https://doi.org/10.1111/srt.12353 https://onlinelibrary.wiley.com/doi/pdf/10.1111/srt.12353

Anthonissen, M., Kerckhove, E., Moortgat, P., Geraerts, I., Devoogdt, N., De Vrieze, T., De Groef, A.: Can the CutiScan CS 100® measure anisotropy and viscoelasticity in scar tissue after mastectomy? a reliability and validity study. Skin Research and Technology **28**(2), 246–253 (2022) https://doi.org/10.1111/srt.13120

Elouneg, A., Lucot, Q., Veyrat-Durebex, E., Lejeune, A., Chambert, J., Lihoreau, T., Chatelain, B., Rolin, G., Jacquet, E.: Biomechanical characterization of earlobe keloid by ring suction test. Computer Methods in Biomechanics and Biomedical Engineering **23**(sup1), 99–100 (2020) https://doi.org/10.1080/10255842.2020.1812173

Elouneg, A., Chambert, J., Lejeune, A., Lucot, Q., Jacquet, E., Bordas, S.P.A.: Anisotropic mechanical characterization of human skin by in vivo multi-axial ring suction test. Journal of the Mechanical Behavior of Biomedical Materials **141**, 105779 (2023) https://doi.org/10.1016/j.jmbbm.2023.105779

Elouneg, A.: In vivo mechanical characterization of soft tissues: application to human skin and keloid. PhD thesis, Université Bourgogne Franche-Comté; Université du Luxembourg (2023). https://theses.hal.science/tel-04216822v1

Lucas, B.D., Kanade, T.: An iterative image registration technique with an application to stereo vision. In: IJCAI'81: 7th International Joint Conference on Artificial Intelligence, vol. 2, pp. 674–679 (1981)

Seo, S.: A review and comparison of methods for detecting outliers in univariate data sets. PhD thesis, University of Pittsburgh (2006)

Rahrovan, S., Fanian, F., Mehryan, P., Humbert, P., Firooz, A.: Male versus female skin: what dermatologists and cosmeticians should know. International Journal of Women's Dermatology **4**(3), 122–130 (2018) https://doi.org/10.1016/j.ijwd.2018.03.002

Dao, H., Kazin, R.A.: Gender differences in skin: A review of the literature. Gender Medicine **4**(4), 308–328 (2007) https://doi.org/10.1016/S1550-8579(07)80061-1

Leveque, J., Corcuff, P., Rigal, J., Agache, P.: In vivo studies of the evolution of physical properties of the human skin with age. International Journal of Dermatology **23**(5), 322–329 (1984) https://doi.org/10.1111/j.1365-4362.1984.tb04061.x

Shuster, S., Black, M.M., McVitie, E.: The influence of age and sex on skin thickness, skin collagen and density. British Journal of Dermatology **93**(6), 639–643 (1975) https://doi.org/10.1111/j.1365-2133.1975.tb05113.x

Olsen, L.O., Jemec, G.: The influence of water, glycerin, paraffin oil and ethanol on skin mechanics. Acta Dermato-Venereologica **73**(6), 404–406 (1993) https://doi.org/10.2340/0001555573404406

Taylor, R.: Interpretation of the correlation coefficient: A basic review. Journal of Diagnostic Medical Sonography **6**(1), 35–39 (1990) https://doi.org/10.1177/875647939000600106

Gräßel, D., Prescher, A., Fitzek, S., Keyserlingk, D.G., Axer, H.: Anisotropy of human linea alba: A biomechanical study. Journal of Surgical Research **124**(1), 118–125 (2005) https://doi.org/10.1016/j.jss.2004.10.010

Lin, C.-Y., Sugerman, G.P., Kakaletsis, S., Meador, W.D., Buganza, A.T., Rausch, M.K.: Sex- and age-dependent skin mechanics—a detailed look in mice. Acta Biomaterialia **175**, 106–113 (2024) https://doi.org/10.1016/j.actbio.2023.11.032

A Clinical Trial Subjects

Table 1: Information on age, sex, and skin thickness for all subjects. Volunteer numbers were assigned based on the sum of the epidermis (th_{e}) and dermis (th_{d}) thicknesses, sorted in ascending order. Additional details about each volunteer and measurement conditions, including daily activity, preferred hand, temperature, and humidity, are documented in the experiment logs, available at: https://dmarc.femto-st.fr/fichiers/822/arborescence. Notes: (1) All subjects were Caucasian except for "006," who had dark skin. (2) Subjects "003" and "008," aged above 50, were excluded and replaced by "031" and "032." (3) All subjects were right-handed except for "002," "015," and "023.

Volunteer	SKUM code	Sex	Age	th_{e} [μm]	th_{d} [μm]
1	026	Female	20	203	703
2	001	Female	32	219	734
3	029	Female	35	203	781
4	019	Female	26	203	797
5	025	Female	20	201	890
6	022	Female	24	203	891
7	013	Female	47	188	906
8	017	Female	33	203	891
9	009	Female	30	220	875
10	020	Female	32	250	859
11	027	Female	26	188	938
12 ($S_{\mathrm{w}1}$)	006	Female	26	180	953
13 ($S_{\mathrm{w}2}$)	005	Female	25	109	1031
14	016	Female	42	156	984
15	023	Female	26	141	1000
16	011	Female	48	172	984
17	032	Female	23	125	1032
18	012	Female	25	172	1000
19	024	Female	25	250	938
20	014	Female	30	250	938
21	031	Female	23	188	1031
22	028	Female	24	344	891
23	018	Female	24	172	1094
24 ($S_{\mathrm{w}3}$)	002	Male	49	188	1094
25	030	Male	22	188	1094
26 ($S_{\mathrm{w}4}$)	007	Male	45	203	1109
27	021	Male	24	219	1109
28	015	Male	38	156	1219
29	010	Male	39	188	1219
30 ($S_{\mathrm{w}5}$)	004	Male	29	203	1266

B Anisotropy Axis Assessment

Table 2: Values of the mean, median, and standard deviation of the anisotropy axis orientation (ϕ) assessed across 21 pressure levels for 30 series conducted on volunteers $S_{\mathrm{w}1}$, $S_{\mathrm{w}2}$, and $S_{\mathrm{w}3}$. (*) Series discarded due to $\mathrm{SD}_{\mathrm{mp}} > 4.5,^{\circ}$ and a discrepancy between the mean and median exceeding $4.5,^{\circ}$. (**) The series discarded because its mean value was identified as an outlier among the 30 series.

Volunteer	$S_{\mathrm{w}1}$			$S_{\mathrm{w}2}$			$S_{\mathrm{w}3}$		
Series	Mean [°]	Median [°]	$\mathrm{SD}_{\mathrm{mp}}$ [°]	Mean [°]	Median [°]	$\mathrm{SD}_{\mathrm{mp}}$ [°]	Mean [°]	Median [°]	$\mathrm{SD}_{\mathrm{mp}}$ [°]
1	85.9 (**)	86.1	2.3	4.4	4.5	0.8	27.4	27	2.1
2	13.3	13.4	3.7	9.8	10.1	1.8	23	22.7	1.6
3	26.2	25.9	1.5	10.3	10.3	2.1	23.3	23.2	1.1
4	26.9	26.9	0.9	3.2	3.3	0.9	33.4	33.4	3.3
5	23	23.1	1.8	4.1	4.2	0.8	33.2	32.7	3.8
6	14.7	15.3	2.5	24.7	24.8	1.4	17.3	17.2	1.7
7	10.1	10	1.6	-3.4	-3.6	0.9	19.8	20.1	1.9
8	16.1	15.6	1.5	-1.7	-2	1.8	35.1	35.3	1.9
9	28.9	29.7	2.2	16.3	16.2	0.8	35.4	36.1	3.3
10	21.2	20.5	3.1	22.8	23.1	2	33	32.6	2.2
11	28.1	28.1	2.5	29.9	30.3	1.8	45.1	45.2	3.1
12	-10.8 (*)	-5.2	18.5	-9.7	-9.6	0.8	28.6	28.6	1.1
13	26.1	26	0.4	10.6	10.9	2.4	21.7	21.6	1.5
14	21.4	21.5	1.1	14.1	14	0.8	22.3	22.3	1
15	21	21.1	1.5	39.2	38.7	1.7	25.4	28.3	6.4
16	21.8	22.1	1.1	8.4	7.9	4.8	59.4	56.5	14.9
17	31.1	30.6	2.8	16.9	16.4	1.1	44.3	45.2	9.2
18	23.7	23.8	0.7	13.4	13.4	0.4	22.3	23	2.2
19	13.9	13.9	1.1	10.5	10.5	2	30.3	30.3	0.9
20	22	22.2	0.7	13.6	13.6	0.6	36.4	36	1.5
21	12	11.8	1.6	10.3	10	1.5	30.7	31.3	4.6
22	39.2	40.1	1.9	17.5	17.4	1.5	27.1	27	1.6
23	18.7	18	1.9	13.4	13	1.4	21.1	20.4	4.8
24	20.2	19.7	1.5	26.3	26.9	1.2	40.6	40	5.5
25	16.9	17.1	3.1	5.8	6.2	2.7	22.9	24.3	3.3
26	21	20.7	1.6	14.2	14.2	0.6	39.9	42.2	6.4
27	6.7	6.7	0.8	29.5	28.4	5.8	19	18.4	3.3
28	28.3	28.4	13.2	17.3	17.1	2.2	20.6	21.3	3.1
29	15.7	15.7	1.9	26.9	27.2	1.7	28.6	25.8	10.8
30	21.4	20.2	3.3	9.3	9.6	1.9	14.7	14.7	2.2

Table 3: Values of the mean, median, and standard deviation of the anisotropy axis orientation (ϕ) assessed across 21 pressure levels for 30 series conducted on volunteers $S_{\mathrm{w}4}$, and $S_{\mathrm{w}5}$. (**) The series discarded because its mean value was identified as an outlier among the 30 series.

Volunteer	$S_{\mathrm{w}4}$			$S_{\mathrm{w}5}$		
Series	Mean [°]	Median [°]	$\mathrm{SD_{mp}}$ [°]	Mean [°]	Median [°]	$\mathrm{SD_{mp}}$ [°]
1	24.3	24.5	2.8	68.2	66.7	9.4
2	35.3	34.2	8.2	52.8	52.9	8
3	19.1	20.5	2.7	57.8	57.8	1.2
4	23.8	23.7	6.5	63.1	63.1	4.8
5	33.6	33.9	2.6	52	50.5	7.9
6	26	25.6	2.2	56.2	55.8	2.7
7	21.6	21.7	1	62.2	65.4	9.3
8	26.8	26.7	1.8	24.8	25.5	2.4
9	28.4	28.7	3.5	46.7	47	2.9
10	16.4	18.3	3.8	63.3	62.7	3.6
11	29.2	29.4	1	59.1	58.8	2.5
12	26.4	26.9	1.6	49.8	49.4	3.7
13	31.1	31.1	1.8	45	45.2	1.9
14	16.2	15.8	2	69.4	68.4	11.9
15	21	21.6	1.4	45.9	46.1	1.5
16	29.9	30	1.3	65.1	64.9	2.8
17	32.7	31.4	2.9	42.8	42.1	6
18	8.7	8.5	0.9	60.7	63.5	8.5
19	36.6	36.5	4.8	56	55.5	6.5)
20	9.2	9.8	1.4	62.4	62.2	2.1
21	12.6	12.5	1.8	41.3	41.4	6
22	9.6	10	1.8	66.4	66.9	3.7
23	14	14.6	2.9	59.1	58.4	3
24	17.1	17.6	4	100.6 (**)	100.5	2.9
25	19.6	19.8	1.9	48.9	49.8	13.2
26	19.7	19.3	2.3	48.3	48.1	0.7
27	18.4	17.4	3.6	38.6	39.1	4.1
28	29.5	29.3	1.3	61.4	60.6	3.2
29	8.9	9	2.3	48	48.2	2
30	15.8	16.8	3.4	66.4	66.2	5.3

Table 4: Values of the mean, median, and standard deviation of the anisotropy axis orientation (ϕ) assessed across 21 pressure levels for 3 series conducted on all volunteers except $\{S_{\mathrm{w}1}, S_{\mathrm{w}2}, S_{\mathrm{w}3}, S_{\mathrm{w}4}, S_{\mathrm{w}5}\}$.

Volunteer	Day 1			Day 2			Day 3		
	Median [°]	Mean [°]	$\mathrm{SD_{mp}}$ [°]	Median [°]	Mean [°]	$\mathrm{SD_{mp}}$ [°]	Median [°]	Mean [°]	$\mathrm{SD_{mp}}$ [°]
1	25.9	25.8	0.9	15.5	16.3	3	16	15.8	2.6
2	23	22.5	4	26.2	26	3.9	20.5	20.9	3.5
3	9.2	9.1	1.5	11	10.9	0.6	29.3	29.7	1.9
4	31.1	31.3	1	15.2	15.4	2.5	26.7	27.1	1.8
5	20	19.8	0.7	9.8	9.9	0.7	19.5	19.4	1.4
6	27	27.3	0.9	26.3	26.2	1.1	32.9	34.7	4.2
7	11.9	11.9	0.4	-0.4	-0.8	1.8	0.2	0	1.3
8	27.7	27.5	1.1	22.5	22.9	1.4	22.3	22.4	0.5
9	17.9	18.2	2	-0.4	-0.4	1.7	7.2	7	1
10	16.9	17.2	3	19.4	20.1	1.9	12.9	13.6	2
11	16	17.3	2.3	23.7	23.9	1.2	15	15.2	1.4
14	33.2	33.1	2.6	39.7	39.5	3.7	35.5	35.5	1.5
15	16.5	16.6	1	17.7	18	1.8	13.3	13.4	0.7
16	25.2	24.5	1.5	15.3	16.3	4.9	33.5	33.5	1.8
17	21.2	20.9	3.4	11.6	12.7	3.7	28.8	30.2	3.3
18	12	13.7	4.6	17	17.3	1.4	18.3	19.6	7.5
19	-6.8	-4.4	8.4	15.7	15.6	1.5	13.7	13.8	1.4
20	22.8	22.6	1.4	59.5	58.7	4.5	37.1	36.1	4.6
21	53.9	54.4	1.3	43.4	43.5	0.5	8.9	8.9	1.5
22	28	27.9	1.1	38.6	38.4	1.8	41.7	41	4
23	39.2	38.7	3.6	14.9	14.3	2.1	33.5	33.4	1.6
25	38.6	38.8	3.7	42.4	43.6	2.7	31.6	31.5	5.7
27	24.4	27.1	6.6	37	36.2	4.4	33.6	33.8	2.3
28	43.3	43.1	3	38.6	39.1	2.3	16.6	17.8	3.6
29	58.9	60.1	6.2	24.9	26.1	4.1	31.7	32.5	2.8

C Uncertainty Analysis of Measurement Across Cumutaltive Series

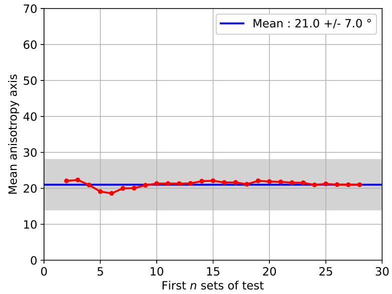

(a) $S_{\mathrm{w}1}$

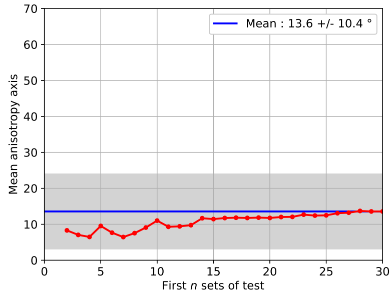

(b) $S_{\mathrm{w}2}$

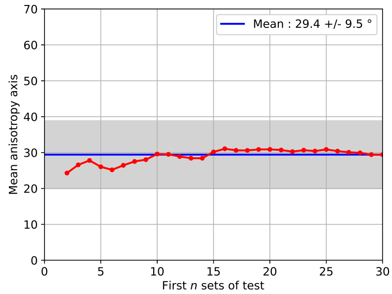

(c) $S_{\mathrm{w}3}$

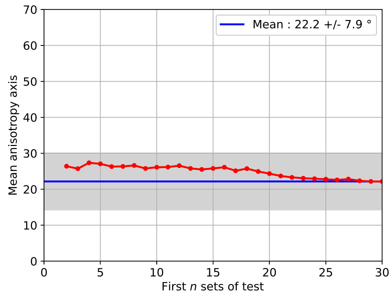

(d) $S_{\mathrm{w}4}$

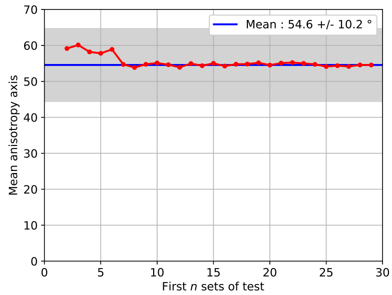

(e) $S_{\mathrm{w}5}$

Fig. 9: Comparison of the mean anisotropy axis value, ϕ, averaged over the entire set of mechanical measurement series ($n \approx 30$, solid blue line) versus the mean value of ϕ averaged over the first n subsets (red dotted line). The light grey area represents the 95% confidence interval, with its width corresponding to the standard deviation of the full set.

D Analysis of Differences in Sample Sizes

Due to the imbalance in the sample size (23 females versus 7 males), the results regarding statistical disparity may not be conclusive. To further investigate this limitation, we employed the same statistical methods to evaluate the discrepancy between the entire male sample ($n = 7$) and all possible combinations of 7 females drawn from the pool of 23, resulting in 245157 comparisons. In 96% of these cases, the sampled subgroups were normally distributed, and variance homogeneity was confirmed in 100% of cases. As shown in Figure 10, 77% of the comparisons revealed a significant difference (p-value < 0.05) between the two groups of equal size.

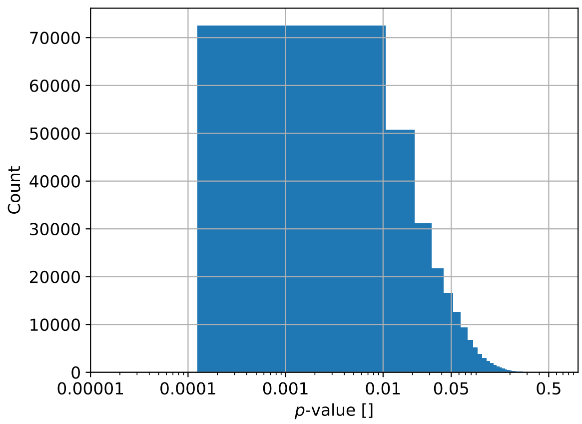

Fig. 10: Statistical evaluation of the discrepancy between female and male with equal sample size for all the 245157 combinations. The proportion of the total surface area represented by values below 0.05 is 77%, an observation that may not be obvious due to the logarithmic scale employed on the X-axis.

E Skin structure's effect in the anisotropic behavior

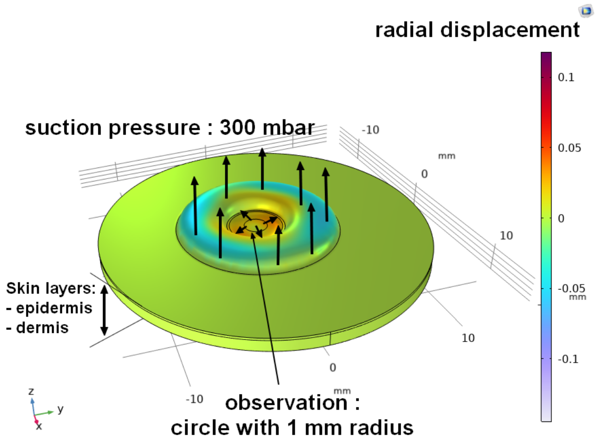

(a) $S_{\mathrm{w}2}$

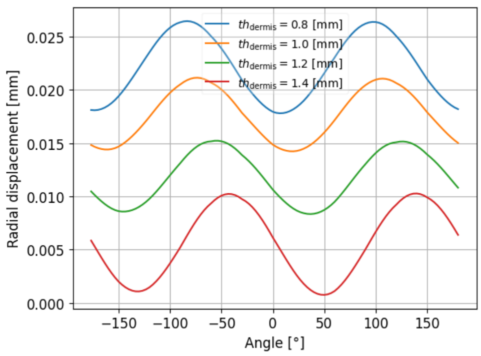

(b) $S_{\mathrm{w}3}$

Fig. 11: Illustration of the relationship between skin structure and anisotropic behavior through numerical simulations conducted in COMSOL Multiphysics. The model consists of 50 k quadratic tetrahedral elements and includes two layers: the epidermis with a fixed thickness of 0.2 mm, and the dermis with varying thickness configurations of th_{dermis} 0.8, 1.0, 1.2, and 1.4 mm. Both layers are modeled as incompressible, Hookean, transverse isotropic materials, with elastic parameters selected to match the mechanical response observed in our clinical trial results. For the epidermis, the anisotropy axis is aligned at $0\,°$, with Young's moduli of $E_1 = 10$ MPa (along the anisotropy axis) and $E_2 = 5$ MPa (across the axis). For the dermis, the anisotropy axis is oriented at $60\,°$, with $E_1 = 2$ MPa, and $E_2 = 1$ MPa. The resulting global anisotropy axis angles correspond to the dips in the curves shown in (b).